Mechanics of Composite Materials, Vol. 36, No. 2, 2000

INTERLAMINAR FRACTURE AND LOW-VELOCITY IMPACT OF CARBON/EPOXY COMPOSITE MATERIALS[1]

J. H. Hwang, O. Kwon, C. S. Lee, and W. Hwang

Keywords: *carbon/epoxy composites, interfacial ply orientation, crack propagation direction, interlaminar fracture, strain energy release rate, low-velocity impact, residual energy, delamination, ultrasonic inspection*

The interlaminar fracture and the low-velocity impact behavior of carbon/epoxy composite materials have been studied using width-tapered double cantilever beam (WTDCB), end-notched flexure (ENF), and Boeing impact specimens. The objectives of this research are to determine the essential parameters governing interlaminar fracture and damage of realistic laminated composites and to characterize a correlation between the critical strain energy release rates measured by interlaminar fracture and by low-velocity impact tests. The geometry and the lay-up sequence of specimens are designed to probe various conditions such as the skewness parameter, beam volume, and test fixture. The effect of interfacial ply orientations and crack propagation directions on interlaminar fracture toughness and the effect of ply orientations and thickness on impact behavior are examined. The critical strain energy release rate was calculated from the respective tests: in the interlaminar fracture test, the compliance method and linear beam theory are used; the residual energy calculated from the impact test and the total delamination area estimated by ultrasonic inspection are used in the low-velocity impact test. Results show that the critical strain energy release rate is affected mainly by ply orientations. The critical strain energy release rate measured by the low-velocity impact test lies between the mode I and mode II critical strain energy release rates obtained by the interlaminar fracture test.

Introduction

Fiber-reinforced polymer composites have been extensively used as fundamental structural members in various engineering fields because of their superior mechanical characteristics such as strength-to-weight, stiffness-to-weight, and fatigue resistance compared to other materials. Polymer composite materials, however, have some serious limitations. In particular, fiber-reinforced laminates are very susceptible to interlaminar fracture and transverse impact, especially at mode I/II fracture and low-velocity impact [1-3].

Fiber-reinforced composites, unlike isotropic materials, have relatively complicated fracture mechanisms. In general, the fracture damage modes are fiber breakage, matrix cracking, interface debonding, and delamination. Among these modes, the major forms of interlaminar fracture and impact damage are matrix cracking and delamination [4]. Delamination occurs with fracture at the interface when adjacent plies are of different orientations and are subjected to interlaminar normal and shear stresses. Apparently, the interlaminar shear stress and the in-plane transverse tensile stress are the dominant stresses causing the critical matrix cracking. Delamination is usually of a peanut shape, and the longitudinal axis of the delamination tends to orient itself parallel to the

[1] Submitted to the 11th International Conference on Mechanics of Composite Materials (Riga, June 11-15, 2000).

Department of Mechanical Engineering, Pohang University of Science and Technology (POSTECH), Pohang 790-784, Korea: whwang@postech.ac.kr. Published in Mekhanika Kompozitnykh Materialov, Vol. 36, No. 2, pp. 195-214, March-April, 2000. Original article submitted February 22, 2000.

fiber direction of the layer below the delaminated surface [5]. Such damage is very difficult to detect and quantify with the naked eye and can impair the strength and stiffness of the materials. These damages may depend strongly on the interfacial ply orientations and the crack propagation direction, as well as on the thickness of laminates. Since damage initiation and growth involve delamination, the strain energy release rate should be the best parameter for characterizing the impact behavior of composite materials. The strain energy release rate means the fracture energy physically and is also called fracture toughness in the literature.

Many experimental and analytical investigations have been carried out on this topic [1-3, 6-25, 27, 28]. Recent research on interlaminar fracture concentrates on the following topics: fiber bridging phenomena [6-8], the effect of ply orientations on fracture toughness [9], failure mechanism analysis [10], and analytical and theoretical approaches using several FEM methods [11]. Huang and Hull [6] showed that fiber bridging causes a continuous increase in the mode I fracture toughness with increasing crack length in unidirectional glass/epoxy laminates. Russell and Street [7] found that the resistance to delamination extension increased considerably under tensile-dominated loading, due to fiber bridging. They analyzed the effect of temperature and moisture content on the interlaminar fracture toughness. Hwang and Han [8] studied the interlaminar fracture behavior of glass/epoxy laminates under static and cyclic loadings, using a width-tapered double cantilever beam specimen. The recent research on impact can be classified into the following topics: failure mode and mechanism analysis [1, 12-14], parametric study on impact damage [15, 16], comparative analysis of damage [17, 18], and damage measurement methods [2, 3]. Jang et al. [1] examined the relation of the failure mode to the impact loading history for a wide range of fiber/resin composites. Choi et al. [12, 13] conducted the study on low-velocity impact to gain a fundamental understanding of the failure mechanisms and mechanics of fiber-reinforced composites resulting from impact, and to identify the essential parameters governing the impact damage experimentally and analytically. They also analyzed the effect of the stacking sequence, thickness, and impacting mass on the damage of graphite/epoxy laminated composites due to low-velocity impact [15]. Griffin [16] studied the influence of defects, notches, impact damage, and environmental conditions on strength. Lee and Zahuta [17] investigated the growth of impact damage by comparing instrumented impact and static indentation results. Kaczmarek and Maison [18] applied ultrasonics in a comparative analysis of the damage after static indentation and low-velocity impact on a composite with a quasi-isotropic lay-up sequence.

In this study, the interlaminar fracture and the low-velocity impact tests were performed to determine the essential parameters governing the interlaminar fracture and damage of composite materials, using laminated composite specimens with realistic ply orientations and stacking sequences. A further objective is to characterize the correlation of the critical strain energy release rates measured by above two kinds of test. The effect of crack propagation (delamination growth) directions θ and interfacial ply orientations α on the interlaminar fracture toughness was examined with WTDCB and ENF specimens. We assume that θ are 0°, 15°, 30°, and 45°, and α are 0°, 45°, and 90°, respectively. The mode I and mode II critical strain energy release rates (G_{IC} and G_{IIC}) are calculated using the compliance method and the linear beam theory. In the impact test, the effect of ply orientations and thickness of laminated composites on the impact behavior were examined using Boeing impact specimens. Different energy levels were applied to each specimen in the impact event. The residual energy was calculated from the impact test, and the shape and total delamination area were estimated through ultrasonic analysis. The critical strain energy release rate G_C was then calculated.

Theoretical Analysis

Mode I Strain Energy Release Rate. *Compliance Method.* Since the change in the fracture area of WTDCB is a function of the beam taper, we have [8]:

$$C = \delta/P = m_1 a^2 + m_2, \tag{1}$$

$$G_{IC} = -\frac{dU}{dA} = \frac{1}{2} P_C^2 \frac{dC}{dA} = kP_C^2 \frac{dC}{d(a^2)} = km_1 P_C^2, \tag{2}$$

where U is the potential energy, A is the fracture area, C is compliance, P_C is the critical load, δ is the crack opening displacement, a is the crack length, and k is the taper of WTDCB.

Beam Theory. By considering the boundary conditions in the basic differential equation for the deflection of a composite beam under pure flexural loading, the compliance and mode I initial fracture energy are given by [8]

$$C = \frac{\delta}{P} = \frac{12ka^2}{E_x h^3}, \tag{3}$$

$$G_{IC} = kP_C^2 \frac{dC}{d(a^2)} = \frac{12P_C^2 k^2}{E_x h^3}, \tag{4}$$

where E_x is the effective bending modulus of the beam and h is the half-thickness of the specimen.

Mode II Strain Energy Release Rate. *Compliance Method.* Since the change in the fracture area of ENF is $dA = bda$, the compliance and mode II fracture energy are of the form

$$C = \delta/P = m_1 a^3 + m_2, \tag{5}$$

$$G_{IIC} = \frac{1}{2} P_C^2 \frac{dC}{bda} = \frac{1.5 m_1 P_C^2 a^2}{b}, \tag{6}$$

where b is the width of the specimen. The parameter m_1 is the slope of C versus a^3 for the ENF specimen, while m_1 for WTDCB is the slope of C versus a^2.

Beam Theory. Neglecting the influence of shear deformation, we obtain the compliance and mode II critical strain energy release rate of the ENF specimen,

$$C = \frac{2L^3 + 3a^3}{8Ebh^3}, \tag{7}$$

$$G_{IIC} = \frac{9a^2 P_C^2}{16Eb^2 h^3}, \tag{8}$$

where L is the half-span length. The error induced by neglecting the shear deformation may be substantial for large thickness-to-crack length ratios h/a and small shear rigidity [19]. In this study, h/a for ENF is 0.1.

Impact Energy. The impact energy absorption can, in principle, be found by integrating the force-time curves. However, this calculation is extremely sensitive to errors in the measured force. Errors of a few percent in the initial velocity or the force result in hundred percent errors in the calculated energy absorption. This often leads to physically unreasonable energy absorption results. A simple yet accurate method to calculate the impact energy absorption is from the velocity data [17]. The initial velocity v_i is

$$v_i = \sqrt{2gH}, \tag{9}$$

where g is the gravity and H is the drop height. The impact energy absorption E can easily be found as

$$E(t) = E_i - \frac{m}{2} v(t)^2, \tag{10}$$

where E_i is the initial impact energy

$$E_i = \frac{m}{2} v_i^2. \tag{11}$$

The residual energy E_r is defined as

$$E_r = E_{\max} - E_i, \tag{12}$$

where $E_{\max}$ is the maximum absorbed energy.

TABLE 1. Stacking Sequence of Specimens for Interlaminar Fracture Tests

α, deg	θ, deg	Stacking sequence
0	0	$[0^{\circ}_{40}//0^{\circ}_{40}]$
	15	$[0^{\circ}_{24}/15^{\circ}_{4}/0^{\circ}_{8}/-15^{\circ}_{4}//-15^{\circ}_{4}/0^{\circ}_{8}/15^{\circ}_{4}/0^{\circ}_{24}]$
	30	$[0^{\circ}_{24}/30^{\circ}_{4}/0^{\circ}_{8}/-30^{\circ}_{4}//-30^{\circ}_{4}/0^{\circ}_{8}/30^{\circ}_{4}/0^{\circ}_{24}]$
	45	$[0^{\circ}_{24}/45^{\circ}_{4}/0^{\circ}_{8}/-45^{\circ}_{4}//-45^{\circ}_{4}/0^{\circ}_{8}/45^{\circ}_{4}/0^{\circ}_{24}]$
45	0	$[0^{\circ}_{40}//45^{\circ}_{4}/0^{\circ}_{8}/-45^{\circ}_{4}/0^{\circ}_{24}]$
	15	$[0^{\circ}_{24}/15^{\circ}_{4}/0^{\circ}_{8}/-15^{\circ}_{4}//30^{\circ}_{4}/0^{\circ}_{8}/-30^{\circ}_{4}/0^{\circ}_{24}]$
	30	$[0^{\circ}_{24}/30^{\circ}_{4}/0^{\circ}_{8}/-30^{\circ}_{4}//15^{\circ}_{4}/0^{\circ}_{8}/-15^{\circ}_{4}/0^{\circ}_{24}]$
	45	$[0^{\circ}_{24}/45^{\circ}_{4}/0^{\circ}_{8}/-45^{\circ}_{4}//0^{\circ}_{40}]$
90	0	$[0^{\circ}_{40}//90^{\circ}_{4}/0^{\circ}_{8}/90^{\circ}_{4}/0^{\circ}_{24}]$
	15	$[0^{\circ}_{24}/15^{\circ}_{4}/0^{\circ}_{8}/-15^{\circ}_{4}//75^{\circ}_{4}/0^{\circ}_{8}/-75^{\circ}_{4}/0^{\circ}_{24}]$
	30	$[0^{\circ}_{24}/30^{\circ}_{4}/0^{\circ}_{8}/-30^{\circ}_{4}//60^{\circ}_{4}/0^{\circ}_{8}/-60^{\circ}_{4}/0^{\circ}_{24}]$
	45	$[0^{\circ}_{24}/45^{\circ}_{4}/0^{\circ}_{8}/-45^{\circ}_{4}//45^{\circ}_{4}/0^{\circ}_{8}/-45^{\circ}_{4}/0^{\circ}_{24}]$

Note: // — a Teflon insert.

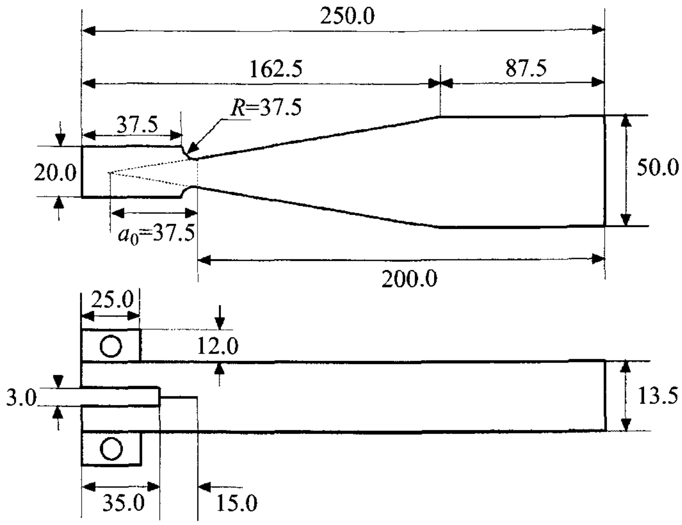

Fig. 1. Geometry of the width-tapered double cantilever beam (WTDCB) specimen with a loading tap (dimensions in mm).

Experimental Procedure

Preparation of Specimens. Carbon/epoxy composite materials, manufactured by Hankuk Fiber Glass Co., were used in this study. This prepreg satisfied DMS (Douglas Material Specification) 2224, type 1, class T, and grade 2. The volume fraction of fibers was 53.3 %.

The width-tapered double cantilever beam (WTDCB) specimens with a taper of 3, for the mode I tests, were machined from 80 layered laminates. These laminates were laid-up by hand, fabricated by autoclave, and cured at 176.7°C (350°F) under 0.7 MPa (100 psi) in accordance with the recommended cure cycle. The stacking sequence of laminates for interlaminar fracture tests is presented in Table 1. Figure 1 shows a schematic configuration of WTDCB. The geometry of WTDCB is based on the results obtained by Hwang and Han [8]. This specimen also satisfies the conditions proposed by Han and Koutsky [20].

The end-notched flexure (ENF) specimens for the mode II tests were manufactured using the same plates and methods as stated above. ENF specimen geometry is shown in Fig. 2. The geometry of ENF, proposed by Carlsson et al. [19, 21], is designed such that h/a (thickness-to-crack length ratio) is 0.1 for linear fracture behavior and a/L (the crack length-to-span ratio) is 0.75 for

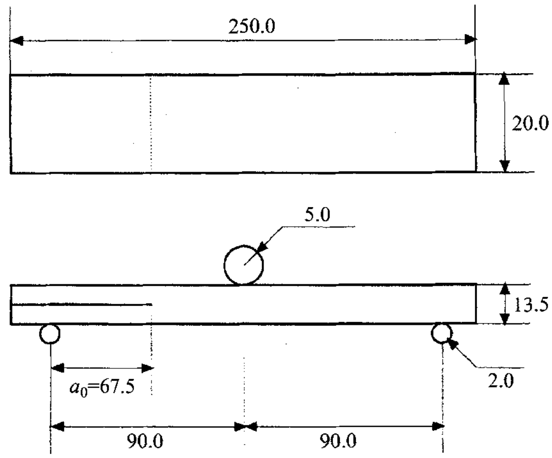

Fig. 2. Geometry of the end-notched flexure (ENF) specimen (dimensions in mm).

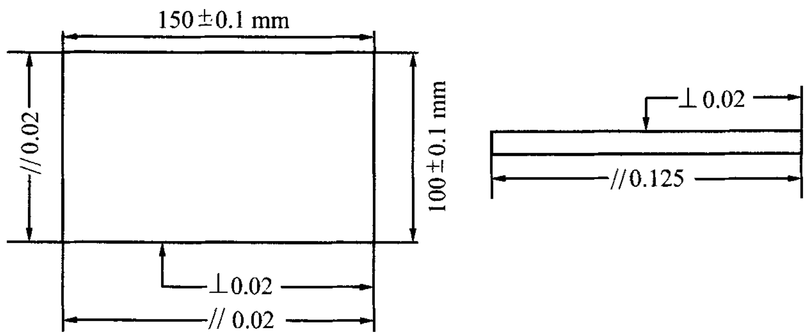

Fig. 3. Geometry of the impact specimen.

stable crack growth. In particular, we use a beam of about 13.5 mm thickness to minimize the nonlinear behavior in the beam such as viscoelastic and plastic deformation effects.

The impact specimens of length 150 mm and width 100 mm, as shown in Fig. 3, each containing equal numbers of 0°, 45°, and 90° plies, were manufactured using the process depicted above. The fiber orientations of specimens with 16 and 32 plies are $[90^\circ_8/0^\circ_8]_s$, $[0^\circ_2/90^\circ_2/0^\circ_2/90^\circ_2]_s$, $[0^\circ_4/-45^\circ_4/90^\circ_4/45^\circ_4]_s$, and $[45^\circ_2/0^\circ_2/-45^\circ_2/90^\circ_2]_s$, from which we can examine roughly the effect of ply orientation and thickness on impact behavior.

Design of Lay-up. Figure 4 shows the definition of the crack propagation direction θ and the interfacial ply orientation α on the midplane. The laminates are designed and fabricated to have an angle α between the upper and lower fiber directions, and an angle θ between the upper fiber direction and the crack propagation direction, in the clockwise sense. Consequently, it is assumed that the crack propagation direction is normal to the crack front formed by a Teflon film and the crack propagates along the midplane. In this paper, θ takes values 0°, 15°, 30°, and 45°, and α is 0°, 45°, or 90°.

In the design of the stacking sequence, we considered three recommendations: the first is to minimize the skewness parameter, the second is to use small-integer $\pm\theta$ plies, and the third is to form a $\theta/-\theta$ sequence. The skewness parameter, suggested by Sun and Zheng [22], is intended to minimize the variation and skewness of the strain energy release rate distribution along the crack front of the specimen, so as to reduce the experimental error. In addition, the number of $\pm\theta$ plies is a small integer in order to reduce the thermal residual stress, and the lay-up is to form a $\theta/-\theta$ sequence in order to eliminate the mode III fracture energy caused by bending-twisting coupling [23]. Therefore, the lay-up sequences are as follows:

$$[0^\circ_{24}/-\theta_4^{(1)}/0^\circ_8/\theta_4^{(1)}//\theta_4^{(2)}/0^\circ_8/-\theta_4^{(2)}/0^\circ_{24}]_T$$

where // indicates the insert location for the artificial precrack.

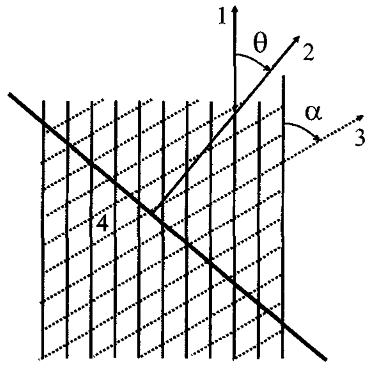

Fig. 4. Definition of the interfacial ply orientation α and the delamination growth direction θ. 1 — orientation of the upper ply, 2 — normal direction to the crack front, 3 — orientation of the lower ply, and 4 — a Teflon film.

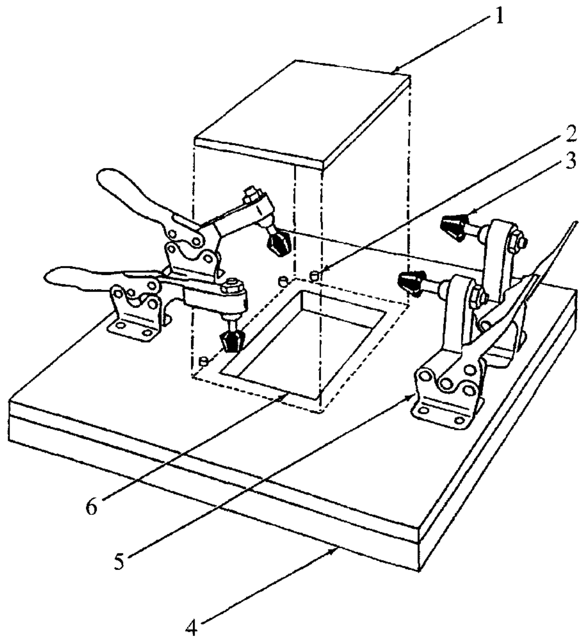

Fig. 5. Boeing test fixture. 1 — 150 × 100 mm pic panel, 2 — guiding tip, 3 — rubber tip, 4 — support base, 5 — clamp, and 6 —125 × 75 mm cut-out.

Experimental Method. We carried out the mode I and mode II interlaminar fracture tests, the low-velocity impact test, and the nondestructive analysis. The interlaminar fracture tests were performed with MTS and UTM test systems. The mode I and mode II tests were conducted at a rate of 1.0 mm/min under displacement control and the crack length measured every 15 sec. In mode I tests, the aluminum loading tap manufactured for the tensile load was attached to the WTDCB using epoxy adhesive, as shown in Fig. 1. The separation between the loading tap and WTDCB specimen did not appear, and this experiment was performed with specially designed grips. Both edges of the specimens were painted with white typewriter correction fluid to make the crack tip more visible. To obtain more accurate results, the experimental procedure took account of the methods/conditions of Hojo et al. [24] and Tanaka et al. [25], including the initial fracture toughness measured at the 5 % offset point and the effect of the starter film.

We also performed low-velocity impact tests using a drop-weight impact tester with a hemispherical nose of diameter 12.7 mm. In this experiment, a Boeing impact test fixture (BSS 7260) was used, as shown in Fig. 5 [26]. As for boundary conditions, the laminated plates were supported by four slap fasteners. The Boeing fixture has a rectangular 125 × 75 mm cut-out. Impact tests were conducted at several impact energy levels, controlled by the impact height, 4.7, 9.4, 14.1, 18.9, 23.6, 33.0, or 42.4 J. The

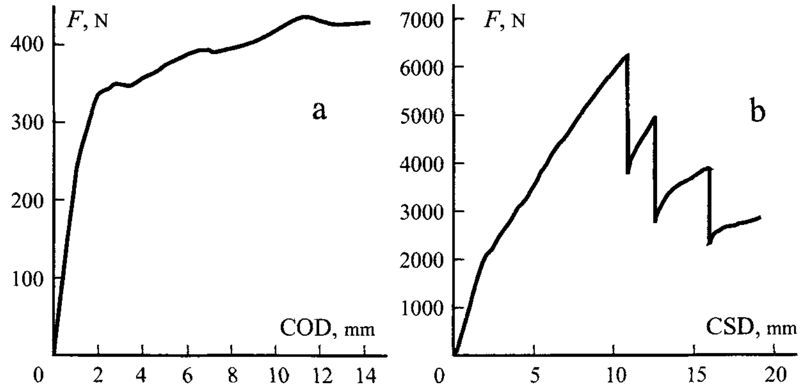

Fig. 6. Typical load-displacement relation: mode I (for the laminate with $\alpha = 90°$ and $\theta = 45°$) (a) and mode II (for the laminate with $\alpha = 90°$ and $\theta = 30°$) (b).

impactor mass was set to 4.807 kg. Restrike of the drop weight was prevented by capturing it after the first impact. The signals from the impact tester were recorded through a LeCroy digital oscilloscope and were amplified by a conditioning amplifier.

The fractured surfaces were observed nondestructively to detect and locate the delamination regions at each interface in the laminated composites. The nondestructive inspection instrument was a SDS 6500 ultrasonic machine (Krautkramer Japan Co.). We used C-scan with the frequency of 80 MHz.

Results and Discussion

Interlaminar Fracture. Typical relations of the load-displacement at interlaminar fracture tests are shown in Fig. 6. The load-crack opening displacement (COD) as a function of the load F for the laminate with $\alpha = 90°$ and $\theta = 45°$ is plotted in Fig. 6a. The critical load is seen to be ~335 N and increases by ~30 % as the crack extends, due to fiber bridging. The fiber bridging, attributed to nesting, where fibers migrate during the curing cycle in unidirectional laminates, increases the critical load and fracture energy by the load transferred to the bridged fibers [8]. While the fiber bridging in angle-ply laminates is caused by crack-tip splitting, this is distinct from the fiber bridging by nesting. Crack-tip splitting occurs in disconnected microscopic subcritical cracks in the region of differently laminated layers immediately in front of the growing crack tip, leading to further bridged fibers in the specimen. It is thought that the change in the critical load due to fiber bridging increases as the interfacial ply orientation or crack propagation angle increases. As shown in the figure, the load increases linearly. But in some regions, the load suddenly decreases because of crack arrest [27]. This phenomenon results from the non-midplane crack propagation by crack-tip splitting, and could be identified by observation of the fractured surfaces in this study. A typical load—crack shear displacement (CSD) curve for the laminate with $\alpha = 90°$ and $\theta = 30°$ is given in Fig. 6b. It is found that the critical load is ~ 2100 N, increases to ~6300 N as the crack extends, and then drops step by step after the fiber breakage by bending, not by shear fracture. The load temporarily decreases owing to the crack arrest as in mode I. Non-midplane crack propagation behavior by sub-critical cracking is also observed.

Figure 7 shows typical trends of the strain energy release rate G_C with increase in the crack length, Δl, in the interlaminar fracture tests. The initial fracture energy (critical strain energy release rate) and crack growth resistance (strain energy release rate) are evaluated by the compliance and beam theory methods. In Fig. 7a, the mode I critical strain energy release rate G_{IC} is ~ 351 J/m^2 by the compliance method and ~ 288 J/m^2 by the beam theory, for the laminate having $\alpha = 90°$ and $\theta = 15°$, and increases as the crack extends. The difference between these values is mainly due to the fiber bridging by nesting and crack-tip splitting and might contain the inaccuracy of the anisotropic beam theory, non-midplane crack propagation behavior, or an experimental error such as the added compliance of the grip [8]. In the mode II interlaminar fracture test, the critical strain energy release rate G_{IIC} is ~ 991 J/m^2 by the compliance method and ~ 875 J/m^2 by the beam theory, for the laminate with $\alpha = 0°$ and $\theta = 30°$, as presented in Fig. 7b. This discrepancy might be due to the inaccuracy of the anisotropic beam theory according to LEFM, the error arising from the neglect of shear deformation, or non-midplane crack propagation behavior by fiber bridging.

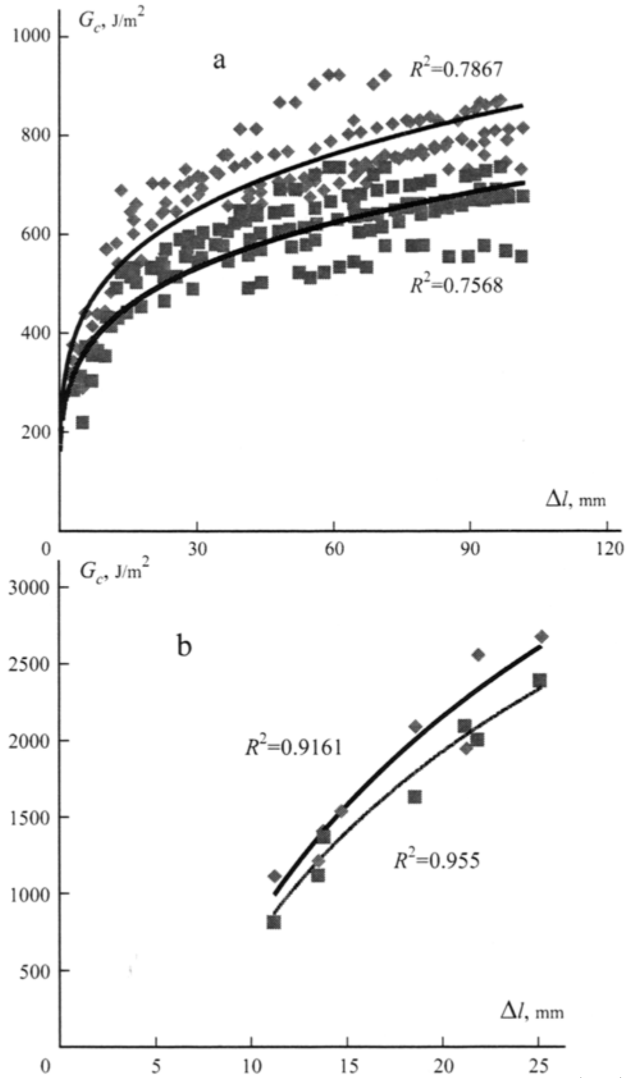

Fig. 7. Typical trends of the strain energy release rate with increase in the crack length in interlaminar fracture tests obtained by the compliance (◆) and beam theory (■) methods: mode I (for the laminate with α = 90° and θ = 15°) (a) and mode II (for the laminate with α = 0° and θ = 30°) (b).

The critical strain energy release rates evaluated by the compliance method and by the beam theory for each mode are summarized in Table 2. The initial fracture energy can be evaluated well by either the beam theory or area methods, while the crack growth resistance due to fiber bridging can be calculated more reasonably by the compliance method [8]. In this study, thus, the critical strain energy release rate evaluated by the beam theory is used in reference to the effect of the crack propagation direction and interfacial ply orientation in each mode. As shown in Table 2, G_{IC} has the maximum values at θ = 15° for the laminates having α = 0°, at θ = 0° for α = 45°, and at θ = 45° for α = 90°. The laminate with α = 45° and θ = = 0° has the maximum value of G_{IC} over all stacking sequences. The G_{IC} of the laminates having α = 45° is much greater than that of the laminates with α = 0° or 90°. These observations might be due to a difference in the bond area between the matrices of differently laminated layers and the change of material properties involved in a variety of ply orientations such as the difference in stiffness of sublaminates, and resistance to delamination growth. G_{IIC} has the maximum values at θ = 0° for the laminates with α = 0°, at θ = 45° for α = 45°, and at θ = 45° for α = 90°. The characteristics of the mode II crack formation mechanism appear to depend on the specimen geometry and material properties, and vary with the difference in lay-up sequences and especially with the fiber direction of the lower subbeam. The G_{IIC} of the

TABLE 2. Mode I and Mode II Critical Strain Energy Release Rates

α, deg	θ, deg	G_{IC}, J/m^2		G_{IIC}, J/m^2	
		Compliance	Beam	Compliance	Beam
0	0	348	302	1419	1417
	15	419	348	1401	1394
	30	414	317	991	875
	45	339	270	762	701
45	0	455	380	915	879
	15	397	363	958	824
	30	385	322	1004	963
	45	426	357	1213	1181
90	0	360	308	631	602
	15	351	288	1059	950
	30	364	311	1089	1005
	45	386	312	1017	1060

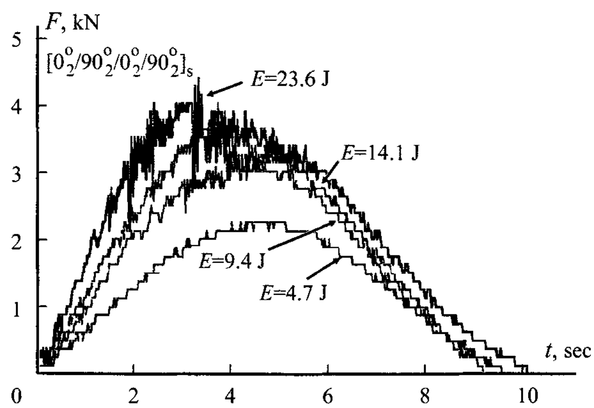

Fig. 8. Force-time curves for various impact energy levels.

laminate having $\alpha = 0°$ and $\theta = 0°$ is of the maximum value in mode II tests. G_{IIC} has much higher values at smaller fiber angles of the lower subbeam for the same interfacial ply orientation on the midplane as a whole. Putting all results together, the critical strain energy release rate is considerably large for the laminate with $\alpha = 45°$ and $\theta = 45°$. The critical strain energy release rate calculated by the compliance method is found to be up to 30 % for mode I and up to 16 % for mode II, greater than the result obtained from the beam theory. The G_{IIC} is 2.0-4.7 times greater than G_{IC}. This is explained by the differing failure mechanisms, sticking features of fracture surfaces, and the extent of plastic deformation of the matrix [10].

Low-Velocity Impact. Figure 8 shows the force F as a function of time t for the $[0^\circ_2/90^\circ_2/0^\circ_2/90^\circ_2]_s$ laminate at various impact energy levels. Independent of the impact energy levels, the impact force initially increases rapidly to a maximum value and then decreases gradually to zero. Under low impact energy levels, the impact force increases linearly and then decreases. As the impact energy increases, the force increases with serious fluctuation. It is found that the starting force resulting in initial damage is independent of the variation in energy levels, and the maximum force increases as the applied impact energy increases. The starting time of the initial damage tends to occur much earlier under high impact energy levels. The fluctuations in the impact force arise from fiber breakage and delamination. These fluctuations are known to distort the real impact behavior.

From the energy-time curve, the energy at the peak force (peak energy), the maximum energy, and the residual energy values are set out in Table 3. On the whole, the panels with more plies have larger values of peak and maximum energies, as expected. The peak and maximum energies for the four panels, except for the residual energy, increase as the energy level increases. As seen

TABLE 3. Energy Values During Impact Loading

Stacking sequence	Energy level, J	Peak energy E_i, J	Maximum energy E_{max}, J	Residual energy E_r, J
$[90^{\circ}_{8}/0^{\circ}_{8}]_s$	14.1	10.845	11.703	0.858
	23.5	19.9	20.669	0.769
	33.0	24.24	25.253	1.013
	42.4	31.872	33.974	2.102
$[0^{\circ}_{2}/90^{\circ}_{2}/0^{\circ}_{2}/90^{\circ}_{2}]_s$	4.7	3.3578	3.4476	0.0898
	9.4	7.3203	7.4323	0.112
	14.1	10.346	11.267	0.921
	18.9	13.231	15.139	1.908
	23.6	15.597	18.628	3.031
$[0^{\circ}_{4}/-45^{\circ}_{4}/90^{\circ}_{4}/45^{\circ}_{4}]_s$	14.1	10.565	11.963	1.398
	23.5	19.373	20.45	1.077
	33.0	24.262	25.128	0.866
	42.4	32.332	33.255	0.923
$[45^{\circ}_{2}/0^{\circ}_{2}/-45^{\circ}_{2}/90^{\circ}_{2}]_s$	4.7	3.2385	3.4855	0.247
	9.4	7.0705	7.3639	0.2934
	14.1	8.7913	11.289	2.4977
	18.9	10.143	15.191	5.048
	23.6	13.894	19.689	5.795

from Table 3, the energy absorption is clearly influenced by the stacking sequence and increases on placing the 45° fiber in the surface plies, as already mentioned by Hitchen and Kemp [28]. The maximum point for energy absorption coincides with the maximum deflection point. Under the same levels of impact energy (for example, energy level of 14.1 J), the maximum energy is roughly constant for all the panels and appears to be independent of the stacking sequence and the thickness of laminates. The maximum energy, in ideal conditions, should be the same as the applied energy level, but in fact is 10 to 15 percent lower because of energy losses. Table 3 indicates that the impact energy is strongly affected by the ply orientation (stacking sequence), which seems to have a greater effect than the laminate thickness. As for the $[0^{\circ}_{2}/90^{\circ}_{2}/0^{\circ}_{2}/90^{\circ}_{2}]_s$ and $[45^{\circ}_{2}/0^{\circ}_{2}/-45^{\circ}_{2}/90^{\circ}_{2}]_s$ laminates, which have the same thickness but different fiber orientations, the residual energy is higher in the $[45^{\circ}_{2}/0^{\circ}_{2}/-45^{\circ}_{2}/90^{\circ}_{2}]_s$ laminate which contains 45° plies. This means that the ply orientation is the major factor in dynamic, such as transverse impact, tests.

Non-destructive testing plays an important role in analyzing the damage of composites by supplying useful information on damage initiation and propagation. The ultrasonic method was applied to delamination detection after a low-velocity impact. From a ply-by-ply ultrasonic analysis, the shape and size of internal damage at each interface were observed and calculated. After impact loading, the damage visualization measured by a C-scan instrument was presented in Fig. 9. The interply delamination shape varied considerably with the stacking sequence and the position penetrated through the thickness [12, 13, 15]. The delaminations generally appeared to be circular or peanut shaped, as shown in Fig. 9. As the impact velocity increased, the increase in delamination length was much greater than that in delamination width.

The maximum and total delamination areas calculated from ultrasonic analysis are listed in Table 4. As the impact energy increases, the delamination area tends to increase, and the increase of impact velocity is more sensitive to the longitudinal length of the delamination area than to the transverse length. Delamination therefore propagates along the longitudinal direction of the fibers. The delamination area tends to increase towards the rear face with increasing distance from the impact site. That is, the results obtained by the ultrasonic method with thickness segment analysis clearly show the propagation of internal delaminations in the case where the delamination areas propagate conically through the thickness. It is found that the maximum delamination area depends on the stacking sequence and the laminates with 45° fibers can resist much larger impact forces. As shown in Tables 3 and 4, the residual energy was found to increase proportionally as the delamination area increases. The residual energy thus can imply the absorbed energy in the propagated delamination.

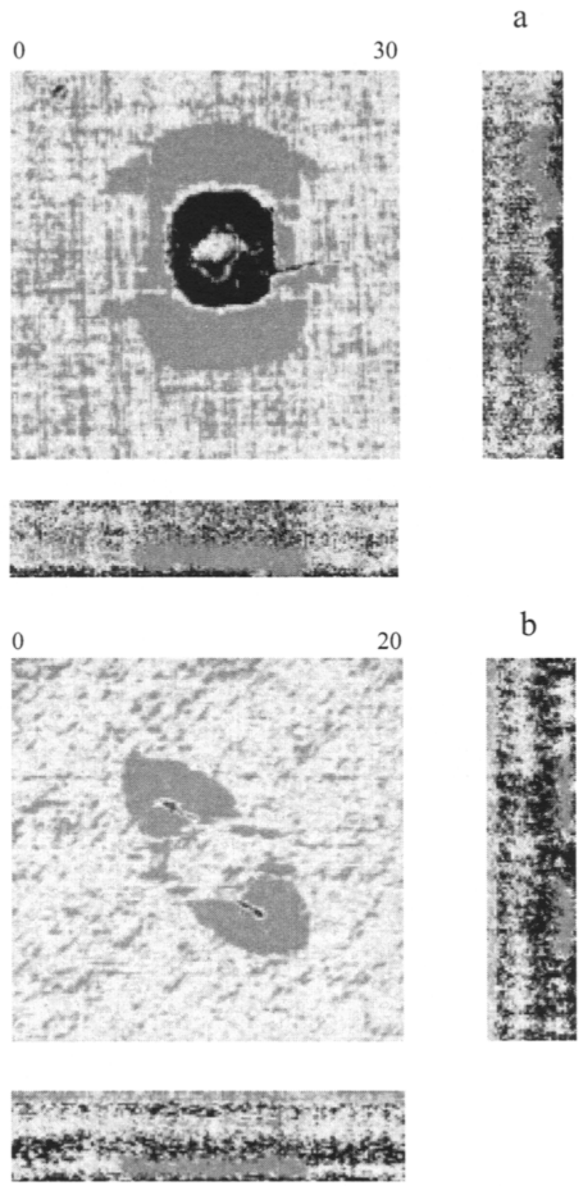

Fig. 9. Damage visualization after impact loading: $[0^\circ_2/90^\circ_2/0^\circ_2/90^\circ_2]_s$ (a) and $[45^\circ_2/0^\circ_2/-45^\circ_2/90^\circ_2]_s$ (b).

The relation between the total delamination area and the residual energy is presented in Fig. 10. Here, the results for $[90^\circ_8/0^\circ_8]_s$ and $[0^\circ_4/-45^\circ_4/90^\circ_4/45^\circ_4]_s$ laminates are absent because there was no visible sign of delamination in these laminates after applying lower impact energy levels of 4.7 J and 9.4 J. The slopes of the straight lines, determined from the experimental data by least squares fitting, correspond to a critical strain energy release rate G_C for delamination extension. The strain energy release rates were found to be 512.5 J/m^2 for $[0^\circ_2/90^\circ_2/0^\circ_2/90^\circ_2]_s$ and 742.1 J/m^2 for $[45^\circ_2/0^\circ_2/-45^\circ_2/90^\circ_2]_s$. The energy threshold may vary for different ply orientations. It was strongly established that the energy release rate is associated with the energy required to initiate the impact damage. This information on the strain energy release rate could be useful in design as a guideline for selecting appropriate composites and for determining the configuration and lay-ups of composite structures in order to sustain impact loads [12].

Correlation between Interlaminar Fracture and Low-Velocity Impact. Since the damage initiation and growth involve delamination, the strain energy release rate or the fracture toughness should be the best parameter for characterizing the impact resistance of composites. However, the fracture behavior under impact cannot be explained by using G_{IC} or G_{IIC} alone because the damage mechanism of impact involves the mode I and the mode II effects concurrently in an unknown ratio. In this study, the critical strain en-

TABLE 4. Delamination Areas with Energy Levels

Stacking sequence	Energy level, J	Delamination area, mm^2	
		maximum	total
$[0^\circ_2/90^\circ_2/0^\circ_2/90^\circ_2]_s$	4.7	43.9	320.3
	9.4	377.0	3015.9
	14.1	820.0	6805.7
	18.9	1272.4	9033.7
	23.6	1866.1	15302.1
$[45^\circ_2/0^\circ_2/-45^\circ_2/90^\circ_2]_s$	4.7	28.1	78.6
	9.4	293.7	895.9
	14.1	728.9	2361.5
	18.9	1206.4	3377.8
	23.6	1792.3	6272.9

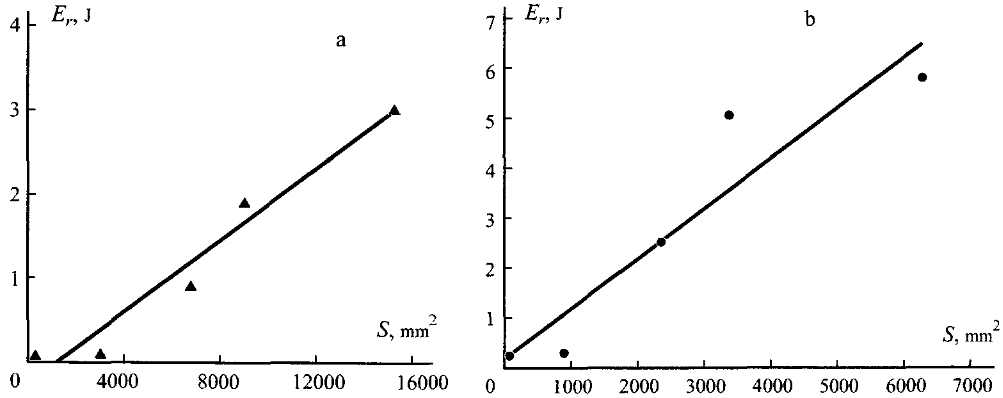

Fig. 10. Relationship between the total delamination area and the residual energy: $[0^\circ_2/90^\circ_2/0^\circ_2/90^\circ_2]_s$, $R = 0.97278$ and $G = 512.47$ J/m^2 (a), $[45^\circ_2/0^\circ_2/-45^\circ_2/90^\circ_2]_s$, $R = = 0.97278$ and $G = 742.07$ J/m^2 (b).

ergy release rate G_C (512.5 J/m^2) estimated from the low-velocity impact test using the $[0^\circ_2/90^\circ_2/0^\circ_2/90^\circ_2]_s$ laminate lies between the critical strain energy release rates (G_{IC} = 308 J/m^2 and G_{IIC} = 602 J/m^2) measured by the interlaminar fracture test using the $[0^\circ_{40}//90^\circ_4/0^\circ_8/90^\circ_4/0^\circ_{24}]_s$ laminate ($\alpha = 90°$ and $\theta = 0°$). The two laminates are of the same ply orientation, though they have different thickness and ratio of the numbers of 0° and 90° plies. Also, the G_C of $[45^\circ_2/0^\circ_2/-45^\circ_2/90^\circ_2]_s$ (742.1 J/m^2) lies between G_{IC} (380 J/m^2) and G_{IIC} (879 J/m^2) of $[0^\circ_{40}//45^\circ_4/0^\circ_8/-45^\circ_4/0^\circ_{24}]_s$ ($\alpha = 45°$ and $\theta = 0°$). It is found that G_C has a more significant correlation with G_{IIC} than with G_{IC}.

Conclusions

The interlaminar fracture and low-velocity impact behavior of carbon/epoxy composite materials have been studied with respect to the effect of interfacial ply orientations, crack propagation directions, and thickness of laminates. The following conclusions are drawn:

1. The critical strain energy release rate calculated by the compliance method is found to be greater than the result obtained from the beam theory. The difference is mainly due to fiber bridging by nesting and crack-tip splitting for the mode I test and fiber bridging by mode I for the mode II fracture.

2. In mode I fracture, the critical strain energy release rate of the laminates having interfacial ply orientation of 45° is much greater than that of the laminates having unidirectional or cross-ply orientations. The mode II critical strain energy release rate has much higher values at smaller fiber angles of the lower subbeam. The difference might be a consequence of the change in the bond area between the matrice and material properties of sublaminates. Collectively, the critical strain energy release rate of the laminate having interfacial ply orientation of 45° and crack propagation direction of 45° is rather high. The mode II critical strain energy release rate is greater than that for the mode I because they have different failure mechanisms.

3. The delamination area, the residual energy, and the strain energy release rate are strongly affected by ply orientations. In particular, laminates containing 45° plies may have a higher delamination threshold.

4. As the impact energy level is increased, the increase in the delamination length is much greater than that in the delamination width. At the same impact energy, the maximum impact energy is independent of the stacking sequence and thickness of laminates.

5. The critical strain energy release rate estimated by the low-velocity impact test lies between the mode I and mode II critical strain energy release rates measured by the interlaminar fracture test. It is found that the critical strain energy release rate has a more significant correlation with the mode II than with the mode I critical strain energy release rate.

Acknowledgment. This research is supported by the Korea Science and Engineering Foundation (KOSEF) under Grant No. 981-1003-021-2. The authors are grateful for this financial support.

REFERENCES

1. B. P. Jang, W. Kowbel, and B. Z. Jang, "Impact behavior and impact-fatigue testing of polymer composites," Compos. Sci. Technol., **44**, 107-118 (1992).
2. H. T. Wu and G. S. Springer, "Measurements of matrix cracking and delamination caused by impact on composite plates," J. Compos. Mater., **22**, 518-532 (June, 1988).
3. H. T. Wu and G. S. Springer , "Impact induced stresses, strains, and delaminations in composite plates," J. Compos. Mater., **22**, 533-560 (June, 1988).
4. B. D. Agarwal and L. J. Broutman, Analysis and Performance of Fiber Composites, 2nd ed., John Wiley & Sons (1990).
5. K. Friedrich (ed.), Application of Fracture Mechanics to Composite Materials, Composite Materials Series. Vol. 6, Elsevier Sci. Publ. (1989), pp. 81-157.
6. X. N. Huang and D. Hull, "Effects of fibre bridging on G_{IC} of a unidirectional glass/epoxy composite," Compos. Sci. Technol., **35**, 283-299 (1989).
7. A. J. Russell and K. N. Street, "Moisture and temperature effects on the mixed-mode delamination fracture of unidirectional graphite/epoxy," in: Delamination and Debonding of Materials, ASTM STP 876 (1985), pp. 349-370.
8. W. Hwang and K. S. Han, "Interlaminar fracture behavior and fiber bridging of glass-epoxy composite under mode I static and cyclic loadings," J. Compos. Mater., **23**, 396-430 (April,1989).
9. R. C. Hudson, B. D. Davidson, and J. J. Polaha, "Effect of remote ply orientation on the perceived mode I and mode II toughness of θ/θ and $\theta/-\theta$ interfaces," Appl. Compos. Mater., **5**, 123-138 (1998).
10. M. D. Gilchrist and N. Svensson, "A fractographic analysis of delamination within multidirectional carbon/epoxy laminates," Compos. Sci. Technol., **55**, 195-207 (1995).
11. S. Liu, Z. Kutlu, and F. K. Chang, "Matrix cracking and delamination in laminated composite beams subjected to a transverse concentrated line load," J. Compos. Mater., **27**, No. 5, 436-470 (1993).
12. H. Y. Choi, R. J. Downs, and F. K. Chang, "A new approach toward understanding damage mechanisms and mechanics of laminated composites due to low-velocity impact. Part I. Experiments," J. Compos. Mater., **25**, 992-1011 (August,1991).
13. H. Y. Choi, H. T. Wu, and F. K. Chang, "A new approach toward understanding damage mechanisms and mechanics of laminated composites due to low-velocity impact. Part II. Analysis," J. Compos. Mater., **25**, 1012-1038 (August, 1991).
14. M. M. Sohi, H. T. Hahn, and J. G. Willaims, "The effects of resin toughness and modulus on compressive failure modes of quasi-isotropic graphite/epoxy laminates," in: Toughened Composites, ASTM STP 937 (1987), pp. 37-60 .
15. H. Y. Choi, H. S. Wang, and F. K. Chang, "Effect of laminate configuration and impactor's mass on the initial impact damage of composite plates due to line-loading impact," J. Compos. Mater., **26**, No. 6, 804-827 (1992).

16. C. F. Griffin, "Damage tolerance of toughened resin graphite composites," in: Toughened Composites, ASTM STP 937 (1987), pp. 23-33.
17. S. M. Lee and P. Zahuta, "Instrumented impact and static indentation of composites," J. Compos. Mater., **25**, 204-222 (February, 1991).
18. H. Kaczmarek and S. Maison, "Comparative ultrasonic analysis of damage in cfrp under static indentation and low-velocity impact," Compos. Sci. Technol., **51**, 11-26 (1994). S. P. Joshi and C. T. Sun, "Impact-induced fracture in a quasi-isotropic laminate," J. Compos. Technol. Res., **9**, No. 2, 40-53 (1987).
19. L. A. Carlsson, Jr., J. W. Gillespie, and R. B. Pipes, "On the analysis and design of the end notched flexure (ENF) specimen for mode II testing," in: G. M. Newaz (ed.), Delamination in Advanced Composites, Tech. Publ. Co. (1991), pp. 204-214.
20. K. S. Han and J. Koutsky, "The interlaminar fracture energy of glass fiber reinforced polyester composites," J. Compos. Mater., **15**, 371-388 (July, 1981).
21. L. A. Carlsson, J. W. Gillespie, and B. R. Trethewey, "Mode II interlaminar fracture of graphite/epoxy and graphite/PEEK," J. Reinf. Plast. Compos., **5**, 170-187 (July, 1986).
22. C. T. Sun and S. Zheng, "Delamination characteristics of double-cantilever beam and end-notched flexure composite specimens," Compos. Sci. Technol., **56**, 451-459 (1996).
23. Y. Li, S. Li, J. Xiao, and J. Tao, "Study on the mode I interlaminar fracture toughness of multi-directional laminates," in: Proc. of ICCM-11. Vol. II. Fatigue, Fracture and Ceramic Matrix Composites, Australia, 14th-18th July (1997), pp. 431-437.
24. M. Hojo, K. Kageyama, and K. Tanaka, "Prestandardization study on mode I interlaminar fracture toughness test for CFRP in Japan," Compos., **26**, No. 4, 243-255 (1995).
25. K. Tanaka, K. Kageyama, and M. Hojo, "Prestandardization study on mode II interlaminar fracture toughness test for CFRP in Japan," Composites, **26**, No. 4, 257-267 (1995).
26. BOEING Specification Support Standard BSS 7260, Advanced Composite Compression Tests, Danatup/General Research Corporation.
27. K. Tohgo, Y. Hirako, H. Ishii, and K. Sano, "Mode I interlaminar fracture toughness and fracture mechanism of angle-ply carbon/nylon laminates," J. Compos. Mater., **30**, No. 6, 650-661 (1996).
28. S. A. Hitchen and R. M. J. Kemp, "The effect of stacking sequence on impact damage in a carbon fibre/epoxy composite," Composites, **26**, No. 3, 207-214 (1995).